International Journal of Pressure Vessels and Piping 187 (2020) 104154

Contents lists available at ScienceDirect

International Journal of Pressure Vessels and Piping

journal homepage: http://www.elsevier.com/locate/ijpvp

Effects of dilution on the hardness and residual stresses in multipass steel weldments

Y.L. Sun [a,b,*], C.J. Hamelin [c,d], A.N. Vasileiou [e], Q. Xiong [a], T.F. Flint [a], G. Obasi [f], J.A. Francis [a], M.C. Smith [a]

[a] Department of Mechanical, Aerospace and Civil Engineering, School of Engineering, The University of Manchester, Sackville Street, Manchester, M13 9PL, UK
[b] Welding Engineering and Laser Processing Centre, School of Aerospace, Transport and Manufacturing, Cranfield University, Cranfield, MK43 0AL, UK
[c] ANSTO, Institute of Materials Engineering, New Illawarra Road, Lucas Heights, NSW, 2234, Australia
[d] EDF Energy, Barnett Way, Barnwood, Gloucester, GL4 3RS, UK
[e] Dalton Nuclear Institute, The University of Manchester, Sackville Street, Manchester, M13 9PL, UK
[f] Department of Materials, School of Natural Sciences, The University of Manchester, Sackville Street, Manchester, M13 9PL, UK

ARTICLE INFO

Keywords:
Fusion welding
Molten mixture
Phase transformation
Hardness
Residual stress
Modelling

ABSTRACT

A thermal-metallurgical-mechanical model was developed to study the effects of dilution in each weld pass for multipass gas tungsten arc and submerged arc welding in low alloy steel (i.e. SA508) plates. Hardness distributions and residual stresses were measured on the transverse sections perpendicular to the welding direction of the manufactured weldments. The predicted hardness and residual stresses were compared with the measurement data and shown to be reasonably accurate. The results showed that dilution can significantly affect both the hardness and the residual stress field in the weld metal. It was found that, for the base and filler materials used, increased dilution led to greater weld-metal hardness and reduced the magnitude of tensile stress or promoted compressive stress in the as-deposited and reheated weld metals. This mechanical behaviour is associated with the tendency for diluted weld metal to experience delayed austenite decomposition, owing to the high hardenability of SA508 steel relative to the filler materials used. Although dilution is irrelevant for the hardness of the base material and its transformation products adjacent to the weld metal, it affected the full-field residual stresses via the equilibrium interaction between the stresses in the base and weld metals.

1. Introduction

The mechanical properties of welds and the residual stresses in weldments have significant effects on structural integrity, and thus they are of particular concern for safety-critical structures such as those found in nuclear reactor pressure vessels [1,2]. Key properties of welds, such as strength and toughness, require optimisation to enhance their in-service performance and prolong their service life. As weld residual stresses are usually detrimental to service life owing to their adverse effects on fatigue, creep, fracture and environmentally assisted cracking [1–3], they need to be mitigated or managed accordingly [2,4]. Unfortunately, the mitigation of weld residual stress is difficult and expensive for large structures (e.g. nuclear reactor pressure vessels and steam generators), and it is often necessary to consider these stresses in structural integrity assessments [5].

Manufacture of thick-section structures (e.g. nuclear reactor pressure vessels) still relies on multipass arc welding [1,6]. Welding gives rise to a non-uniform transient field of temperature ranging from ambient temperature to melting point and beyond, and consequently, the microstructure of a weldment is inevitably heterogeneous due to the evolutionary metallurgical processes (e.g. dilution, grain growth, phase transformation and in-process tempering [7–11]) that are controlled in part by the applied thermal load. Since mechanical properties (e.g. yield strength and fracture toughness) are strongly dependent on microstructure, it is necessary to evaluate the resultant heterogeneity of mechanical properties in the fusion zone (FZ) and heat affected zone (HAZ) of a weldment [12–14]. Regarding weld residual stress, its origin and development in ferritic steel weldments are complicated by multi-physics factors, which include the thermal expansion mismatch, transformation-induced deformation and plastic distortion.

* Corresponding author. Department of Mechanical, Aerospace and Civil Engineering, School of Engineering, The University of Manchester, Sackville Street, Manchester, M13 9PL, UK.
E-mail addresses: yongle.sun@manchester.ac.uk, sunyongletl@gmail.com, Yongle.Sun@cranfield.ac.uk (Y.L. Sun).

https://doi.org/10.1016/j.ijpvp.2020.104154
Received 1 October 2019; Received in revised form 5 July 2020; Accepted 13 July 2020
Available online 18 July 2020

The effects of dilution on the mechanical behaviour of a multipass steel weld arise from the following two mechanisms. First, dilution affects the chemical composition of weld metal, assuming that a chemical mismatch between the base and filler materials exists. The alloying elements have a primary impact on the final microstructures developed within either the as-deposited weld metal or the reheated weld metal during subsequent weld passes, as commonly occurs in multipass welding processes. The microstructures that were influenced by dilution determine the mechanical properties of the diluted weld. Second, dilution leads to distinctive solid-state phase transformation (SSPT) kinetics in weld metals produced by different passes. The final residual stress field, which is known to be influenced by SSPT kinetics [1,15–17], is thus affected by dilution.

Previous experimental studies [18,19] have demonstrated the effects of dilution on the mechanical properties (e.g. hardness and toughness) of single-pass welds. However, the effects of dilution are further complicated when the weld metal experiences several transformation cycles during multipass welding. The experimental investigation [20] of residual stresses in multipass steel welds indicates that dilution significantly affects the stress state of the welds made of low transformation temperature filler alloys, due to the sensitivity of martensite start temperature to the chemical composition of the diluted weld [17]. However, dilution is often neglected in multipass weld modelling [16,21,22], despite recent research efforts to clarify its effects [23–25]. The oversight of dilution may introduce significant errors in the predicted SSPT kinetics and thus leads to elevated uncertainty in modelling results. Therefore, the effects of dilution on the mechanical behaviour of multipass welds require further quantification and clarification.

This paper is concerned about the effects of dilution on the hardness and residual stresses in multipass arc weldments made of SA508 steel. The investigation into effects of dilution on the alloy content and microstructure of the arc weldments identical to these studied here has been reported in a previous paper by the same authors [24]. As yield strength is generally proportional to hardness [26], the effect of dilution on yield strength is expected to be similar to that for hardness. In Section 2, the welding experiments and the methods of measurement and modelling for hardness and residual stresses are described. In Section 3, the experimental and modelling results are presented. The discussion and conclusions are presented in Section 4 and Section 5, respectively.

2. Materials and methods

2.1. SA508 steel weldments

SA508 Gr. 3 Cl. 1 steel was used in the preparation of experimental weldments, including three (i.e. 1-pass, 2-pass and 3-pass) welded plates produced using gas tungsten arc (GTA) welding process and three (i.e. 1-pass, 2-pass and 3-pass) welded plates produced using submerged arc (SA) welding process. All plates have dimensions of 30 × 170 × 300 mm, and the 1-pass and 2-pass welded plates were produced using the same process parameters as the 3-pass welded plate. A through-length U groove was machined from each plate; for the GTA welded plates, the depth and width of the groove were 6 mm and 15 mm, respectively, while for the SA welded plates, the groove dimensions were 10 mm and 16 mm, respectively. It should be mentioned that the groove geometry chosen here was consistent with other grooved and narrow-gap welded specimens studied elsewhere within the same research programme [6] and the main research purpose here is to understand dilution effects rather than to produce weldments with perfectly filled grooves. The GTA welding heat input and torch travel speed were 1.57–1.97 kJ/mm and 75 mm/min, respectively; for SA welding, these values were 0.81 kJ/mm and 450 mm/min, respectively. More details about the parameters of weld process and geometry can be found in Ref. [24].

The carbon equivalent has been calculated using the Ito-Bessyo equation [27,28]:

$$C_{eq} = C + Si/30 + (Mn + Cu + Cr)/20 + Ni/60 + Mo/15 + V/10 + 5B \quad (1)$$

where the symbols denote the weight percentages of chemical elements. Table 1 shows the chemical compositions of base and filler materials, and the C_{eq} values are 0.30, 0.22 and 0.17 for the base material, GTA and SA weld fillers, respectively.

The chemical composition of the weld metal produced by each pass can be calculated using a dilution-based rule-of-mixtures, as follows

$$p_n = p_b D_n + p_f (1 - D_n) \quad (2)$$

where D_n is the dilution for n-th pass (Table 2); and p_n, p_b and p_f are the weight percentages of each chemical element for the n-th pass weld metal, the base and filler materials, respectively. The calculated chemical composition of weld metal generally agrees well with experimental measurement [24]. Apart from the differences in the dilution and chemical compositions of the weld metals for the two welding processes, the SA welding process gave rise to higher cooling rate than the GTA welding process, as shown in Table 2, mainly due to the lower heat input of the SA welding process.

2.2. Experimental measurements

Micro-hardness measurements based on the Vickers method were performed using a Durascan tester with an applied load of 1 kgf, and a series of test matrices were constructed with predefined test points for 2D mapping of hardness distribution. The distance between different test points (primarily located in the weld region) ranged from 0.35 mm to 0.5 mm for the three GTA weld samples, which were cut from the 1-pass, 2-pass and 3-pass GTA welded plates. The distance between test points ranged from 0.3 mm to 1.5 mm for the three SA weld samples, which were cut from the 1-pass, 2-pass and 3-pass SA welded plates. All the samples were extracted as transverse-section slices far from the weld ends. The hardness measurement data were then plotted as 2D contour maps using the Matlab software (R2014a).

The incremental centre-hole drilling (ICHD) method was employed to measure the near-surface residual stress on the weld centreline for the 3-pass GTA and SA welded plates. The ICHD technique is semi-invasive, which determines the residual stress based on the measurements of relieved strains due to hole drilling, along with the subsequent calculations using a series of equations [29]. The ICHD measurements were performed by VEQTER Ltd., UK. The welded plates were cut into two halves through the mid-lenght plane for microstructure characterisation [24]. Then two locations at the weld centreline, with distances of 30 mm (i.e. Measurement A) and 50 mm (i.e. Measurement B) to the mid-length cut plane of the welded plate, were tested in the ICHD measurements. The measurements were carried out by orbital drilling using step increments of 0.05 mm and measurement depth of 1 mm. Strain gauge rosettes of type CEA-06-062UL-120 were utilised, which were designed especially for ICHD measurements and supplied by Vishay Measurements Group UK Ltd. The hole was drilled at the centre of the rosette, with the three-gauge elements being distributed along the circumference of a circle with radius of 2.6 mm. The gauge elements were aligned in the longitudinal, transverse and shear directions. The diameter of the drilled hole was 1.5–2.0 mm.

2.3. Modelling

2.3.1. Hardness prediction

The thermal and metallurgical models for the weld samples studied here have been elaborated in Ref. [24], and thus only the models related to hardness and residual stress are described here. Empirical equations [30–32] that correlate hardness and microstructure are adopted here to predict the impact of the diluted weld microstructure on mechanical properties. The Vickers hardness of a ferritic phase (here refers to ferrite,

Table 1
Chemical compositions (in wt.%) of base and filler materials.

	C	Si	Mn	Ni	Cr	Mo	V	Al	Cu	Ti	Fe
SA508 (base material)	0.16	0.27	1.43	0.77	0.23	0.52	0.003	0.02	0.04	0.003	Bal.
S3 (GTA weld filler)	0.10	0.20	1.47	0.88	0.03	0.25	0.003	0.003	0.075	0.002	Bal.
SDX (SA weld filler)	0.081	0.371	1.481	0.037	0.012	0.003	0.001	0.014	0.054	0.007	Bal.

Table 2
Dilution and cooling rate (^{o}C/s, at 700 °C) for each welding pass [24].

Process	Variable	First pass	Second pass	Third pass
GTA welding	Dilution	0.50	0.27	0.27
	Cooling rate	64 ± 8	63 ± 6	51 ± 6
SA welding	Dilution	0.45	0.24	0.15
	Cooling rate	135 ± 12	118 ± 14	115 ± 9

pearlite, bainite or martensite) is expressed as a function of chemical composition (designated as element symbols in weight percentage) and cooling rate at 700 °C (designated as Vr in ^{o}C/hour) [31], and the expressions are as follows

$$Hv_{\mathrm{M}} = 127 + 949\mathrm{C} + 27\mathrm{Si} + 11\mathrm{Mn} + 8\mathrm{Ni} + 16\mathrm{Cr} + 21\log(Vr) \tag{3}$$

$$Hv_{\mathrm{B}} = -323 + 185\mathrm{C} + 330\mathrm{Si} + 153\mathrm{Mn} + 65\mathrm{Ni} + 144\mathrm{Cr} + 191\mathrm{Mo} + (89 + 53\mathrm{C} - 55\mathrm{Si} - 22\mathrm{Mn} - 10\mathrm{Ni} - 20\mathrm{Cr} - 33\mathrm{Mo})\log(Vr) \tag{4}$$

$$Hv_{\mathrm{F/P}} = 42 + 223\mathrm{C} + 53\mathrm{Si} + 30\mathrm{Mn} + 12.6\mathrm{Ni} + 7\mathrm{Cr} + 19\mathrm{Mo} + (10 - 19\mathrm{Si} + 4\mathrm{Ni} + 8\mathrm{Cr} + 130\mathrm{V})\log(Vr) \tag{5}$$

where Hv_{M}, Hv_{B} and $Hv_{\mathrm{F/P}}$ are the hardness values of martensite, bainite and ferrite/pearlite, respectively. It should be noted that in the hardness calculations the weight percentages of chemical elements in the weld metal are estimated using Eq. (2). The measured hardness of the base material is 200 HV, i.e. $Hv_{\mathrm{b0}} = 200$, and the hardness of retained austenite is approximated to be 80% that of base material [30], i.e. $Hv_{\mathrm{A}} = 160$. Such an approximation of austenite hardness has little effect on the result obtained in present analysis, since a negligible proportion of retained austenite was predicted, in consistence with microscopic observations [24]. The total hardness, Hv, can be calculated using a rule-of-mixtures as follows

$$Hv = Hv_{\mathrm{M}}X_{\mathrm{M}} + Hv_{\mathrm{B}}X_{\mathrm{B}} + Hv_{\mathrm{F/P}}(X_{\mathrm{F}} + X_{\mathrm{P}}) + Hv_{\mathrm{A}}X_{\mathrm{A}} + Hv_{\mathrm{b0}}X_{\mathrm{b0}} \tag{6}$$

where X_{M}, X_{B}, X_{F}, X_{P}, X_{A} and X_{b0} are the fractions of martensite, bainite, ferrite, pearlite, retained austenite and base material, respectively. These phase fractions are obtained using a SSPT kinetics model [30,32] and the metallurgical results have been reported in a previous paper by the same authors [24]. Although strain hardening can be present during welding, its effect on hardness is secondary for SA508 steel [30]. Such a secondary effect becomes even negligible if the weld microstructure is dominated by a brittle phase (e.g. martensite).

The accuracy of Eqs. (3)–(6) has been verified in previous studies on quenching and welding in low alloy steels [32–35], but it should be noted that these equations do not account for the presence of acicular ferrite as observed in some weld metals. In the metallurgical model used here, the transformation kinetics for bainite and acicular ferrite were treated as being equivalent, and only bainite fractions were predicted [24]. Despite the presence of some acicular ferrite in the GTA weld metal [24], Eqs. (3)–(6) were directly applied to calculate the hardness of the GTA weld sample. However, microscopic observations [24] reveal that the SA weld metal is largely acicular ferrite. To take account of this fact, in the analysis case that the actual dilution (Table 2) was used or the dilution was assumed to be zero (pure filler material), the hardness of the predicted bainite in the SA weld metal was approximated to be 214 HV, which is representative for acicular ferrite [36]. By contrast, Eq. (4) was used when the dilution was assumed to be one (i.e. pure base material), which does not involve acicular ferrite [24]. The predicted hardness distributions are compared with the measured 2D hardness maps as a full-field evaluation of the heterogeneous mechanical properties of the weldments.

2.3.2. Stress prediction

The generation of residual stress in a metallic weldment is strongly coupled with the thermo-metallurgical welding process. On one hand, the thermo-metallurgical deformation is the driving force for stress generation; on the other hand, with presence of both stress and SSPT, additional plastic deformation (so-called transformation-induced plasticity [37,38]) can occur at a stress level below the nominal yield strength of the material. This phenomenon has been shown to affect the final weld residual stress field [1,30,39].

Thermal strain is manifested as a volumetric expansion or contraction due to the local change in temperature during welding. Metallurgical strain comprises a volumetric strain component caused by a change in the intrinsic crystal structure and a plastic strain component caused by the presence of a deviatoric stress state during SSPT [1,37,38]. In this study, all thermo-metallurgical strains were calculated in the Abaqus subroutine UEXPAN for stress prediction by a mechanical FE model.

For thermo-metallurgical deformation that is independent of stress, a rule-of-mixtures calculation was performed using the two separate dilatation curves of individual ferritic and austenitic phases, which were calibrated using dilatometry test data for SA508 steel [30]. No distinction in thermal deformation was made between the base and filler materials. Fig. 1 shows the calculated variations of engineering strain with temperature during thermal cycles for both base and filler materials, simulating load-free dilatometry tests. For a given material, different cooling rates are considered, which lead to different metallurgical deformations, due to the effects of cooling rate on SSPT kinetics. For a given cooling rate, the metallurgical deformation occurs at a lower temperature for the base material, as compared to the filler materials, due to the higher carbon equivalent that the base material possesses (Section 2.1).

To capture the transformation-induced plastic strain, the following constitutive equation [40] was used

$$\dot{\varepsilon}_{ij}^{\mathrm{tp}} = \frac{3}{2}Ks_{ij}f'(z)\dot{z} \tag{7}$$

where z is the fraction of a phase transformation product, $\dot{z}$ is the transformation rate, $f(z)$ is a normalised function satisfying $f(0) = 0$ and $f(1) = 1$, s_{ij} is the deviatoric stress, and K is a material constant. The normalised function $f(z)$ describes how the transformation-induced plasticity increases with the increase in the fraction of a transformation product. For SA508 steel, we adopted that $f(z) = z(2 - z)$ and $K = 10^{-4}$ MPa^{-1} [40]. Although the adopted function and constant were determined from experiments on bainite transformation [40], for simplicity they were identically applied to the transformation-induced plasticity for different transformation products considered in the weld model.

The mechanical analysis was carried out after both thermal and metallurgical solutions were obtained, following a sequential coupling modelling approach. Biquadratic, generalised plane strain, hybrid elements (Abaqus designation CPEG8H) were used in the mechanical model, and the nodal coordinates were identical to those used in the corresponding thermal model [24]. The 2D mechanical model is acceptable for estimate of residual stress on a section under steady-state

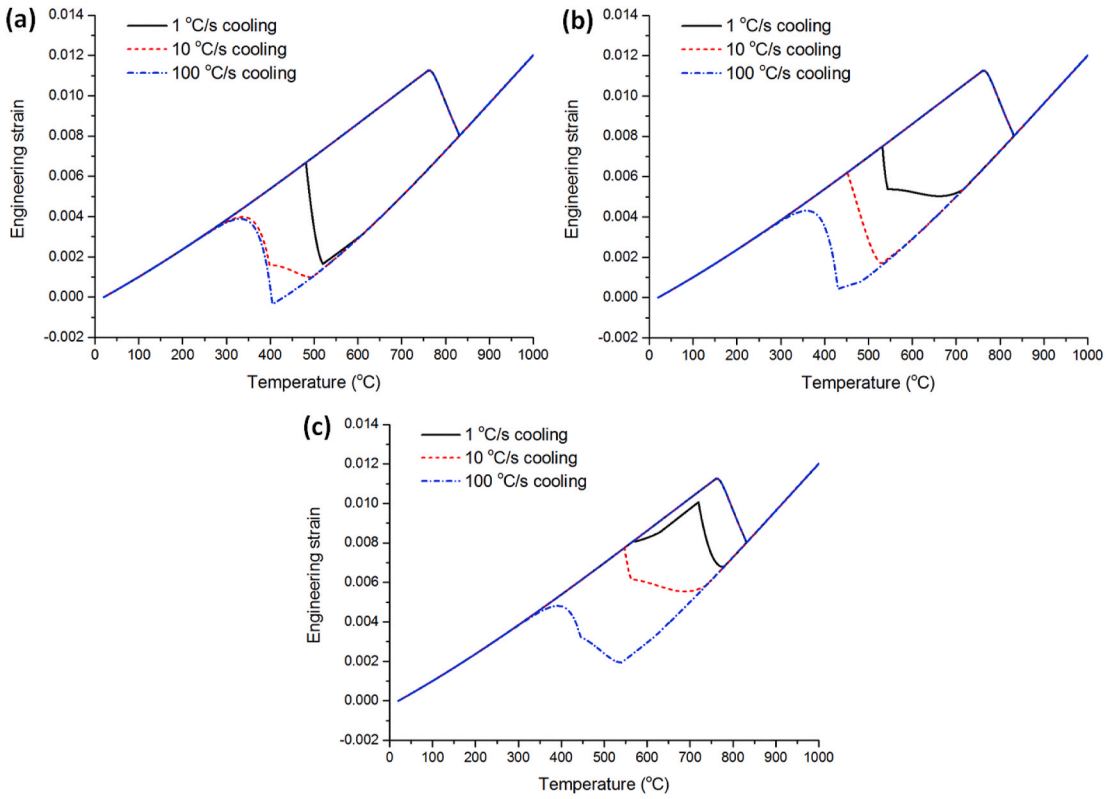

Fig. 1. Calculated variations of engineering strain with temperature during thermal cycles for (a) SA508 Gr. 3 Cl. 1 steel (base material), (b) IABCO™ S3 steel (GTA weld filler) and (c) HOBART™ SDX steel (SA weld filler). A prior austenite grain size of 50 μm was assumed for predicting austenite decomposition kinetics during the dilatometry simulation.

welding conditions [23,41]. To prevent rigid body motion, two nodes on the bottom and close to the middle of the 2D finite element (FE) model were constrained. Fig. 2 shows the FE meshes and boundary conditions.

The material properties used in the FE model are dependent on both temperature and SSPT kinetics. Material parameters for SA508 steel and its transformation products have been reported in Ref. [30], which were adopted in this study. The elasto-plastic properties of the predicted micro-constituents in the weld metal are presumed being same as those of the counterpart transformation products of the base material. The different microstructural phases were indicated through the use of field variables, which were updated in Abaqus subroutine USDFLD, and a rule-of-mixtures was used to estimate the mechanical properties of a mixed microstructure, if any. The Lemaitre-Chaboche strain hardening model was used to capture the plastic behaviour, and the hardening parameters were adopted from Ref. [30].

3. Results

3.1. Hardness

Fig. 3 shows the measured and predicted hardness distributions on the transverse section for the GTA welded plates. It should be noted that dilution only affects the hardness of the weld metal. When the experimentally determined dilution (Table 2) is considered in modelling

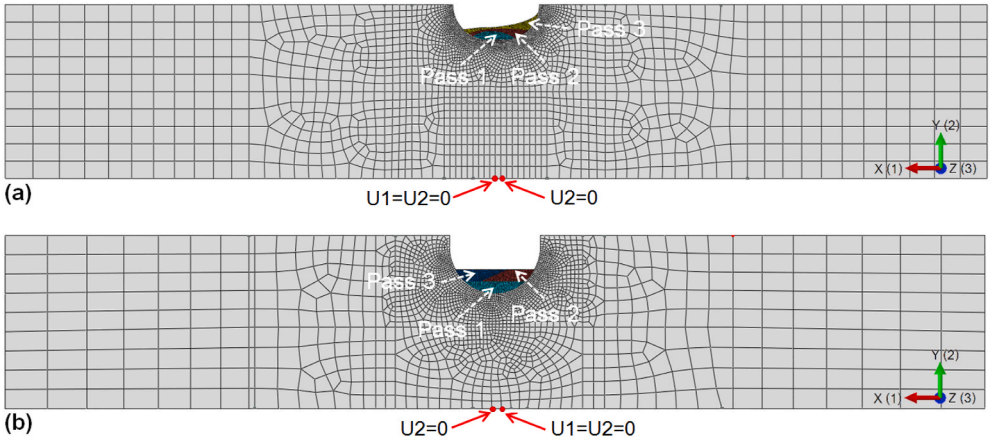

Fig. 2. FE meshes and boundary conditions for mechanical analyses of GTA welding (a) and SA welding (b) in 30-mm thick grooved plates. The out-of-plane length of 300 mm is considered under generalised plane strain assumption. The X (1), Y (2) and Z (3) directions correspond to the transverse, normal and longitudinal directions, respectively.

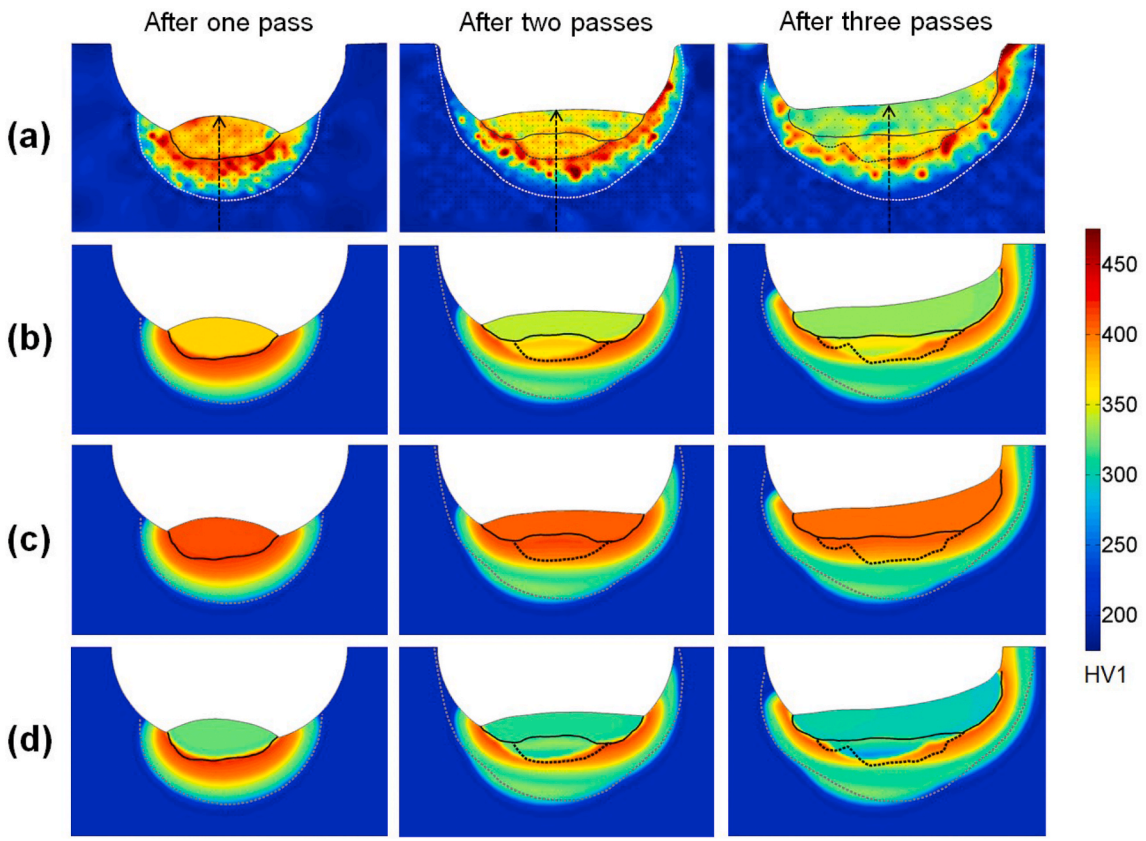

Fig. 3. Comparison between the measurements (a) and predictions (b–d) of hardness distributions in the GTA welded plates. Different scenarios are considered in modelling (D_n indicates the dilution for pass n): (b) $D_1 = 0.5$, $D_2 = D_3 = 0.27$ (experimentally determined); (c) $D_1 = D_2 = D_3 = 1$; (d) $D_1 = D_2 = D_3 = 0$. The black solid line, black dashed line and grey dashed line indicate the boundaries of the current FZ, accumulated FZ and accumulated HAZ, respectively, as observed in macrographs [24]. The path for central line plotting of hardness is indicated by dashed arrow in (a).

(Fig. 3b), the hardness prediction is in good agreement with experimental measurement (Fig. 3a). Unsurprisingly, the coarse-grained HAZ (CGHAZ) that originated in the base material exhibits the highest hardness, as the SA508 steel ($C_{eq} = 0.3$) is more prone to forming martensite when compared against the filler material ($C_{eq} = 0.22$). The CGHAZ in the reheated weld metal, i.e. that formed in the first-pass weld metal after the second and third weld passes, demonstrates a lower hardness than its SA508 counterpart, since the hardenability of the weld metal is relatively low due to limited contribution from the base material. In general, the hardness in both the as-deposited and reheated weld metals decreases when new weld bead is deposited (i.e. from first pass to third pass, see Fig. 3a and b). Fig. 3c and d shows the predictions when the dilution is assumed to be one (i.e. purely base material) and zero (i.e. purely filler material), respectively. It is evident that, when dilution is equal to one, the base-material CGHAZ and weld metal exhibit similar predicted hardness values typical for martensite [24]. By contrast, when dilution is equal to zero, the weld metal exhibits lower predicted hardness values. It can be also seen that there is a slight decrease in overall hardness of weld metal from first pass to third pass, whether dilution is equal to one or zero, which is due to the slight decrease in cooling rate from first pass to third pass (Table 2), thereby promoting the formation of softer phases (e.g. bainite).

Fig. 4 shows the measured and predicted line-profiles of hardness distributions for the GTA welded plates. In Fig. 4 and other following figures where data are plotted as lines, the uncertainty in interpolating the modelling data with high gradient at HAZ/FZ boundary can cause some spikes, while the spikes in measured line-profiles are mainly due to scatter in data between different test points. Lines are taken from the bottom of the plate to the top of the weld cap (Fig. 3a) at a section where steady-state welding conditions are anticipated to exist. The significant effect of dilution can be clearly seen. The assumed dilution values of one and zero are associated with two bounds of the solution, wherein the hardness is overestimated and underestimated by the weld model, respectively. The use of experimentally determined dilution in the weld model leads to hardness predictions that are in best agreement with measurement results. However, it is noteworthy that the predicted hardness in the region that is approximately 20–21 mm away from the bottom surface is substantially higher than the measured hardness after two or three passes. This deviation can be explained by the fact that tempering was not considered in the present model; an over-tempering effect is known to arise near the outer boundary of the HAZ after each pass, which would serve to lower the overall hardness in this region. The tempering effect has been thoroughly investigated in Ref. [9] and thus is not further discussed here.

Fig. 5 shows the measured and predicted hardness distributions for the SA welded plates. The prediction is in reasonable agreement with measurement when experimentally determined dilution is considered in modelling. However, the hardness of the base-material HAZ produced by first pass is overestimated after the second and third passes. This is mainly due to the neglect of tempering effect in the present model, see Ref. [9] for further discussion of tempering effect. Assuming dilution equal to one or zero leads to prediction of hardness dominated by the SSPT behaviour of base material ($C_{eq} = 0.3$) or filler material ($C_{eq} = 0.17$), respectively. As with the GTA welded plates, the hardness in the weld metal is overestimated when a dilution value of one is assumed, and it is underestimated when a dilution value of zero is assumed; i.e. they bound the supposed best-estimate solution. Although the cooling rate of SA welding is approximately twice that of GTA welding (Table 2), the SA weld metal exhibits significantly lower hardness relative to that of the GTA weld metal (Figs. 4a and 5a). Such a result can be attributed

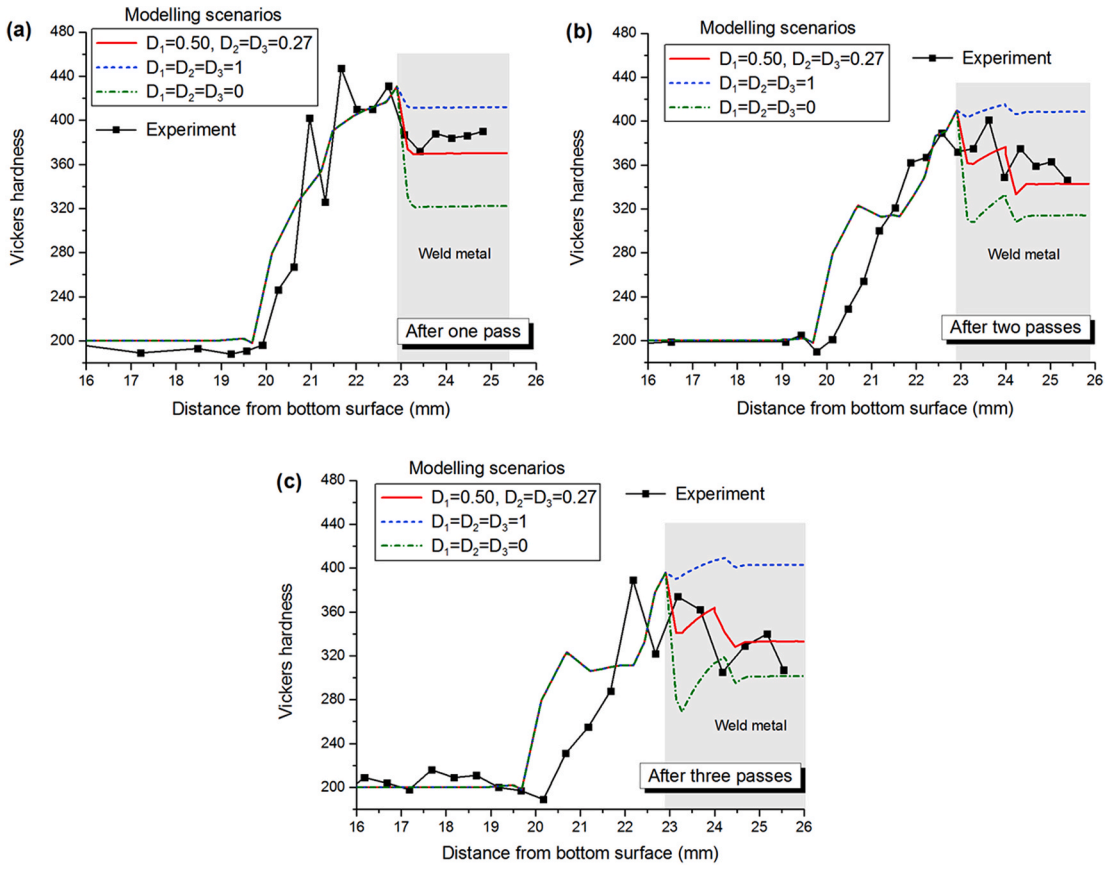

Fig. 4. Line profiles of hardness distributions for the GTA welded plates (see Fig. 3a for the central line path): (a) after one pass; (b) after two passes; (c) after three passes. Note that D_n indicates the dilution for pass *n*.

to the fact that the value of C_{eq} is greater for the GTA weld filler relative to the SA weld filler. Similar to the GTA weld metal, the hardness of the as-deposited SA weld metal decreases with increasing pass. The model has demonstrated the effect of dilution on hardness (Fig. 5b–d). The predicted differences (Fig. 5b) in hardness between weld metal and base-material HAZ, and between weld metals produced by different passes, are consistent with the experimental result (Fig. 5a).

Fig. 6 shows the line profiles of the hardness distributions for the SA welded plates. Since the SA welding process generated a weld region that is not symmetric about the weld centreline, the line paths are selected so as to cover both high and low hardness regions after each pass (Fig. 5a). Also note that both experimental and modelling results show that the as-deposited weld metals produced by successive passes have successively lower hardness values, due primarily to the reduction in dilution pass by pass (Table 2), while the slightly reduced cooling rate (Table 2) in successive pass plays a secondary role; this fact is demonstrated by the similar modelling results for weld metals produced by different passes when dilution values are assumed constant (i.e. one or zero). The dilution effect revealed in Fig. 6 is consistent with the results for the GTA welded plates (Figs. 3 and 4). It should be noted that, even when representative dilution is considered (Figs. 5b and 6), the model systematically overestimates the hardness in the SA weld metal, particularly for the as-deposited weld metal. This issue is associated with acicular ferrite transformation, which will be discussed in Section 4.

3.2. Residual stress

Fig. 7 shows the longitudinal residual stress in the 3-pass GTA welded plate. Fig. 7a–c compares the predicted longitudinal residual stresses when different dilution values are adopted in modelling. In general, high tensile stress is generated around HAZ/base-material boundary. Dilution has not only a direct effect on the weld metal residual stress, but also an appreciable secondary effect for the HAZ and its adjacent base material. This indirect effect arises due to a redistribution of equilibrium stresses, which are caused by the variation of both phase composition and SSPT kinetics in the weld metal. With an assumed dilution of one, low tensile stresses in weld metal and relatively high tensile stresses in the HAZ (Fig. 7b) are predicted. Assuming a dilution value of zero leads to an increase in predicted tensile stresses in the weld metal, and consequently, in the HAZ (Fig. 7c) the tensile stress is reduced while the compressive stress is enhanced, due to the stress equilibrium effect. When experimentally determined dilution is used, an intermediate stress state is predicted (Fig. 7a), which lies between the two bounding cases. The above observation is further verified by comparing the through-thickness distributions of the predicted longitudinal stresses along the weld centreline, as shown in Fig. 7d, in which the ICHD measurement result is also shown. It appears that the measured longitudinal stress in the region with a distance of 50 mm to the mid-length cut plane (i.e. Measurement B) is higher than that for a distance of 30 mm (i.e. Measurement A), presumably due to the increase in constraint with increasing distance to the cut plane (Section 2.2). It is expected that the agreement between the experiment and prediction can be improved when a 3D model accounting for the mid-length cutting before the ICHD measurement is used. Despite the simplification of the 2D model, the prediction accuracy is deemed reasonable at least for a qualitative study.

Fig. 8 shows the dilution effect on transverse residual stress. Again, for dilution equal to one, the weld metal is more prone to compressive stress state; consequently, higher tensile stress is generated in the HAZ. When dilution is set to be zero, the compressive residual stresses in the weld metal relax slightly but the effects are not as significant as for the longitudinal direction, owing to the relatively low mechanical constraint

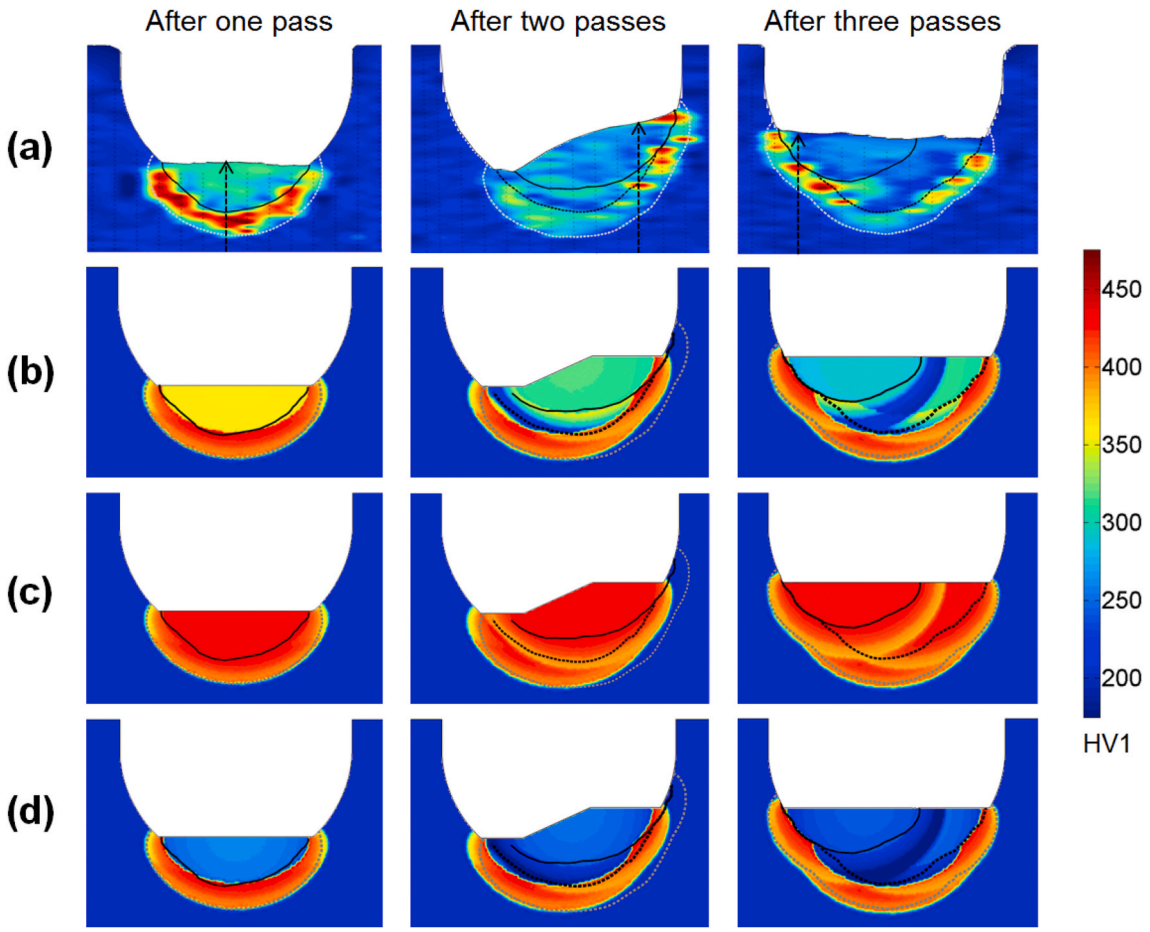

Fig. 5. Comparison between the measurements (a) and predictions (b–d) of hardness distributions in the SA welded plates. Different scenarios are considered in modelling: (b) $D_1 = 0.45$, $D_2 = 0.24$, $D_3 = 0.15$ (experimentally determined); (c) $D_1 = D_2 = D_3 = 1$; (d) $D_1 = D_2 = D_3 = 0$ (D_n indicates the dilution for pass n). The black solid line, black dashed line and grey dashed line indicate the boundaries of the current FZ, accumulated FZ and accumulated HAZ, respectively, as observed in the macrographs [24]. The path for line plotting of hardness is indicated by dashed arrow in (a).

transverse to the weld. For the transverse stress, the measured stress (close to zero) is markedly lower than the predicted stress (Fig. 8d). The uncertainty associated with the ICHD stress measurement on a half plate (Section 2.2) may also be a contributing factor to the discrepancy.

Fig. 9 shows the longitudinal residual stress results for the 3-pass SA welded plate. Fig. 9a–c compares the predicted longitudinal stresses by the model with consideration of different dilution levels. An unsymmetrical stress distribution is obtained, which is consistent with the process asymmetry during the 3-pass SA welding (i.e. the second pass was tilted towards right-hand-side and subsequently the third pass was tilted towards the left-hand-side, so as to complete one filled layer in the groove [24]). High tensile stress is generated in the first-pass HAZ that originated in base material and the weld metal that has not been re-austenitised during the third pass. When dilution is assumed to be one, tensile stresses are reduced in the as-deposited and reheated weld metals, but enhanced in the untransformed weld metal, in contrast to the case that dilution is assumed to be zero. The incorporation of representative dilution in modelling leads to an intermediate stress state between the aforementioned two extreme cases. Such effects of dilution are also clearly seen from the through-thickness line plots of longitudinal stress (Fig. 9d). The agreement between the prediction and measurement is reasonable, as shown in Fig. 9d, although the measured stress exhibits more marked variation in the near-surface region. Again, since the location for Measurement A is less far from the mid-length cut plane, compared to the location for Measurement B (Section 2.2), the measured stress is lower for the former than for the latter.

Fig. 10 compares the predicted transverse stress distributions for different dilution values. The high tensile stress is mainly distributed in the base-material HAZ produced by the first pass. Higher dilution favours the compressive stresses in as-deposited and reheated weld metals and the tensile stress in base-material HAZ. These features are consistent with those of the GTA weldment. The measured transvers stress is close to zero, while considerable compressive stress was predicted by SA weld model, as shown in Fig. 10d, similar to the discrepancy observed in the GTA weldment (Fig. 8d).

4. Discussion

The hardness in the low alloy steel weldment is mainly dependent on the microstructural development during welding. The microscopic observations and metallurgical modelling results for the studied arc weldments, as reported in Ref. [24], revealed that: (1) the base-material HAZ (i.e. the HAZ originated from base material) comprises bainite and martensite; (2) the microstructure of the as-deposited GTA weld metal is a mixture of acicular ferrite, bainite and martensite, in contrast to the dominance of acicular ferrite (with martensite-austenite islands and allotriomorphic ferrite) for the SA weld metal; (3) the reheated weld metal (or weld-metal HAZ) exhibits a microstructure similar to the as-deposited weld metal, despite difference in the fraction of each micro-constituent; (4) increasing dilution promotes martensite but suppresses bainite/ferrite in the weld metal.

The effect of dilution on the weld-metal hardness is significant (Figs. 3–6) and it operates by two mechanisms. Firstly, dilution affects the SSPT kinetics and thus controls the fractions of different micro-

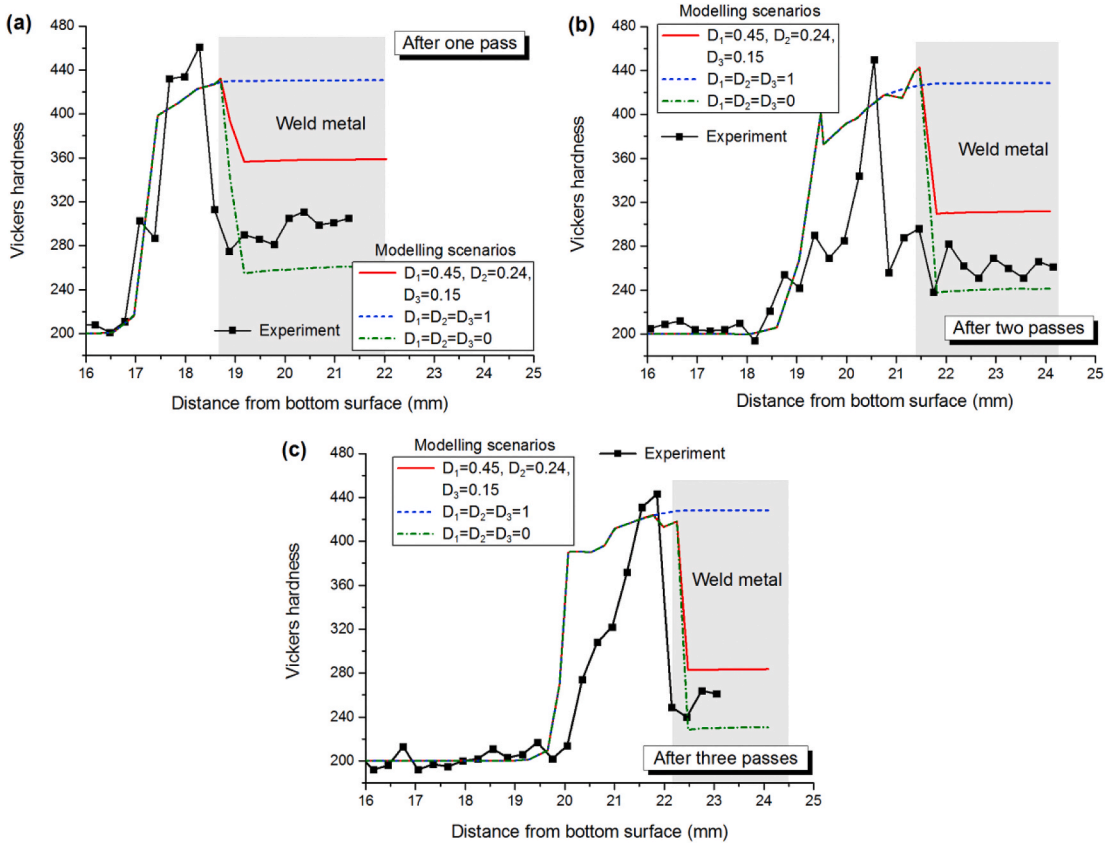

Fig. 6. Line profiles of hardness distributions for the SA welded plates (see Fig. 5a for line path): (a) after one pass; (b) after two passes; (c) after three passes. Note that D_n indicates the dilution for pass *n*.

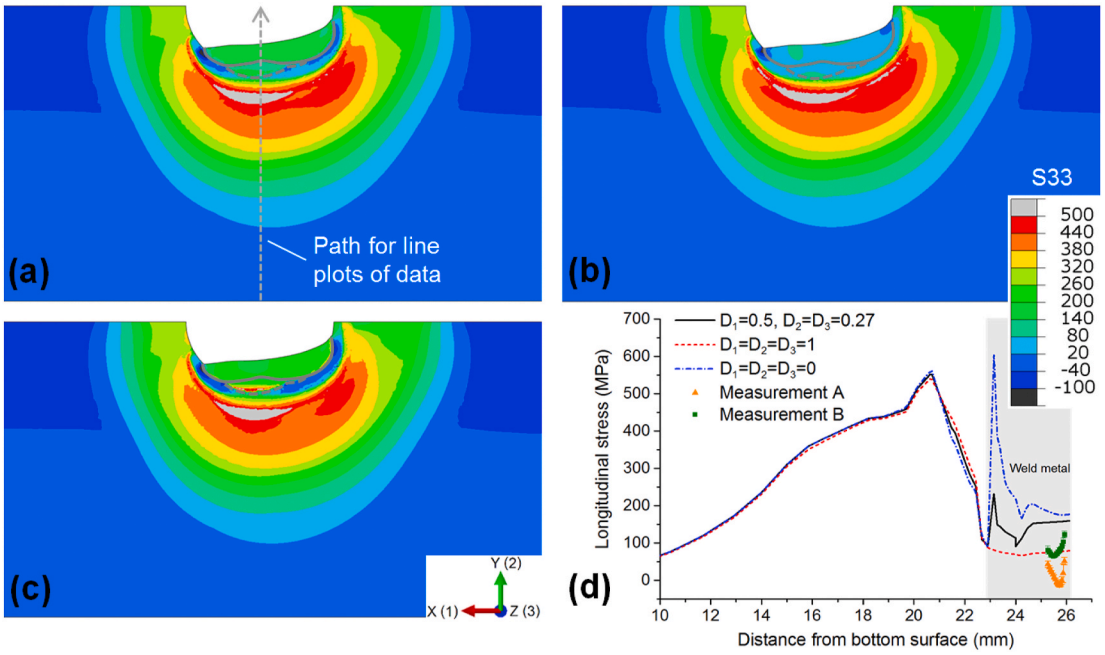

Fig. 7. Longitudinal residual stresses in the 3-pass GTA welded plate: (a) prediction when $D_1 = 0.50$, $D_2 = D_3 = 0.27$; (b) prediction when $D_1 = D_2 = D_3 = 1$; (c) prediction when $D_1 = D_2 = D_3 = 0$; (d) through-thickness distribution along weld centreline. Note that D_n indicates the dilution for pass *n*. Solid and dashed grey lines in (a)–(c) indicate the predicted current and accumulated fusion boundaries, respectively.

constituents (e.g. martensite, bainite and ferrite) formed after cooling; these micro-constituents have different contributions to total hardness (Eq. (6)). Secondly, dilution affects the hardness of each micro-constituent, since the dilution is directly correlated with the chemical composition of weld metal [24] and the hardness is dependent on chemical composition, as shown in Eqs. (3)–(5). However, the second

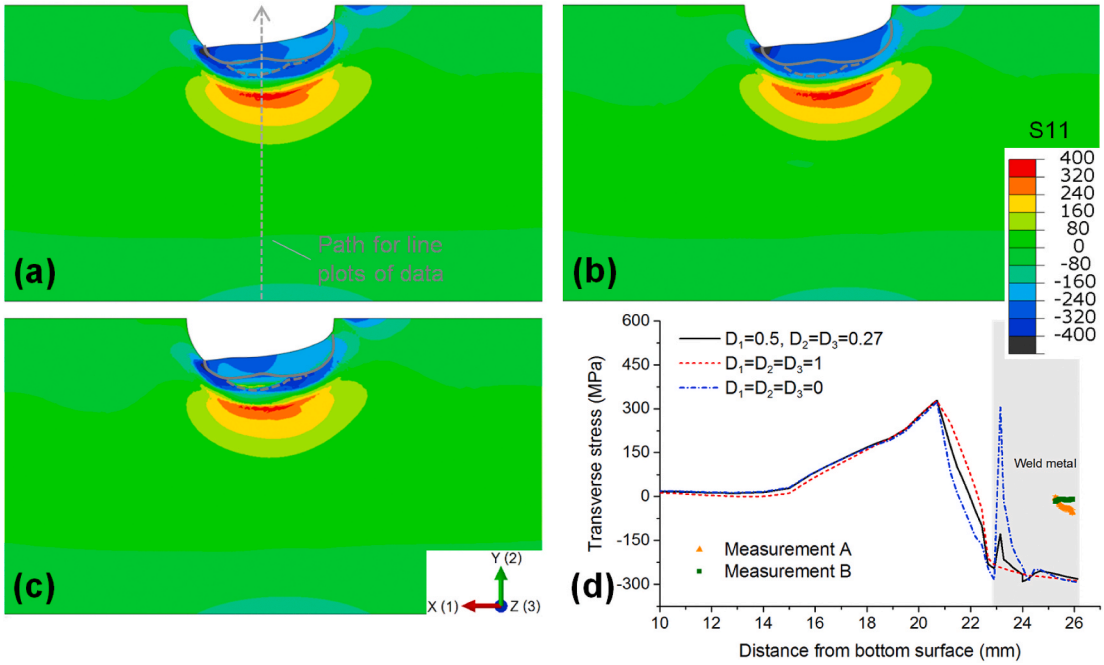

Fig. 8. Transverse residual stresses in the 3-pass GTA welded plate: (a) prediction when $D_1 = 0.50$, $D_2 = D_3 = 0.27$; (b) prediction when $D_1 = D_2 = D_3 = 1$; (c) prediction when $D_1 = D_2 = D_3 = 0$; (d) through-thickness distribution along weld centreline. Note that D_n indicates the dilution for pass *n*. Solid and dashed grey lines in (a)–(c) indicate the predicted current and accumulated fusion boundaries, respectively.

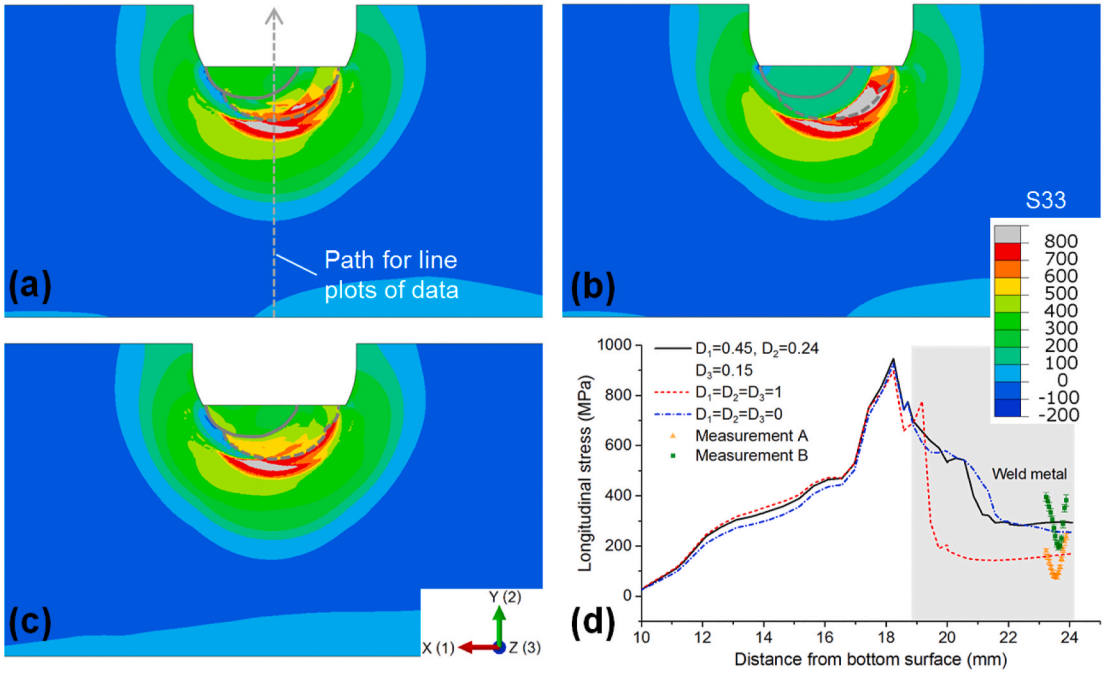

Fig. 9. Longitudinal residual stresses in the 3-pass SA welded plate: (a) prediction when $D_1 = 0.45$, $D_2 = 0.24$, $D_3 = 0.15$; (b) prediction when $D_1 = D_2 = D_3 = 1$; (c) prediction when $D_1 = D_2 = D_3 = 0$; (d) through-thickness distribution along weld centreline. Note that D_n indicates the dilution for pass *n*. Solid and dashed grey lines in (a)–(c) indicate the predicted current and accumulated fusion boundaries, respectively.

effect is usually insignificant unless the chemical mismatch between base and filler materials is exceptionally large. Therefore, the first effect plays a major role in determining the hardness of weld metal studied here. The experimental results (Figs. 3a and 4) for the GTA weldments show that the hardness in the as-deposited weld metal of the 2-pass sample is lower than the 1-pass sample, despite almost identical cooling rate (Table 2), suggesting that the difference is mainly due to dilution effect. The dilution reduced after the first pass (Table 2), and consequently the hardenability of the as-deposited weld metal is lowered by a reduced contribution from the base material which has higher hardenability ($C_{eq} = 0.3$) than the GTA weld filler ($C_{eq} = 0.22$). Similar effect also works for the SA weld-metal hardness (Figs. 5a and 6). The variation in the hardness of as-deposited weld metal between different passes is consistent with the microstructural evolution for both GTA and

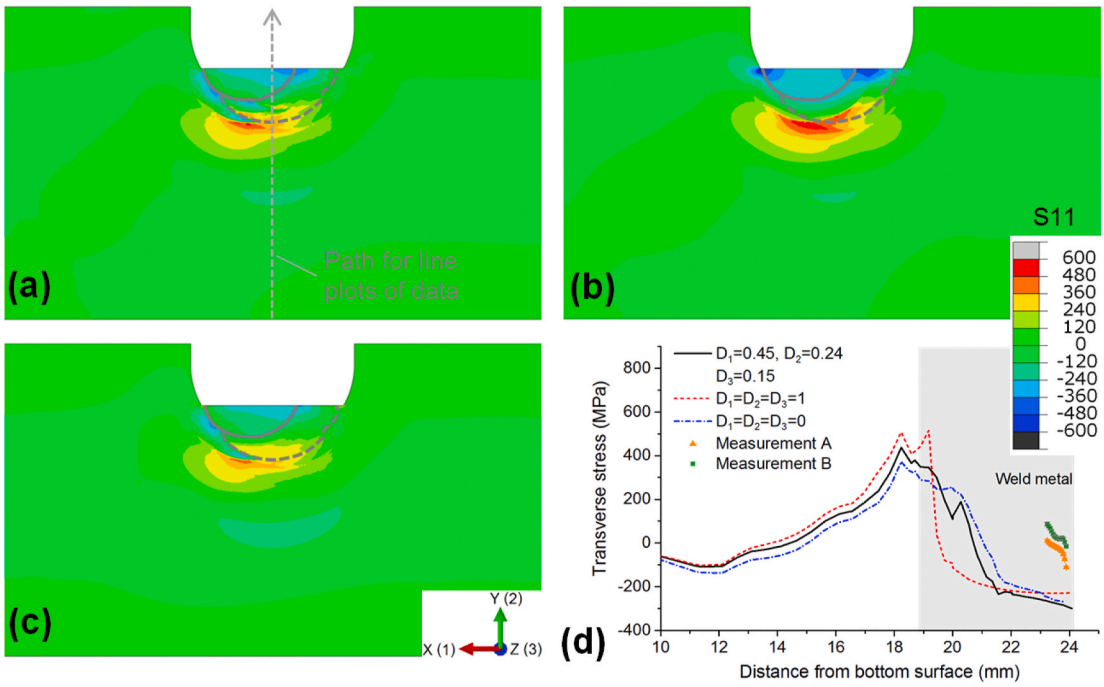

Fig. 10. Transverse residual stresses in the 3-pass SA welded plate: (a) prediction when $D_1 = 0.45$, $D_2 = 0.24$, $D_3 = 0.15$; (b) prediction when $D_1 = D_2 = D_3 = 1$; (c) prediction when $D_1 = D_2 = D_3 = 0$; (d) through-thickness distribution along weld centreline. Note that D_n indicates the dilution for pass n. Solid and dashed grey lines in (a)–(c) indicate the predicted current and accumulated fusion boundaries, respectively.

SA welding processes [24].

For the reheated weld metal, the chemical composition does not change as this material does not re-melt, and thus the hardness is mainly affected by the dilution of the already deposited weld metal (i.e. existing diluted chemical composition before reheating) and the subsequent thermal cycle (i.e. peak temperature and cooling rate). With similar thermal condition during third pass, the third-pass HAZ (i.e. the region close to current FZ) originated from both the base material and the reheated first-pass and second-pass weld metals, wherein the hardness distributions are distinctive, as shown in Figs. 3 and 5, due primarily to the difference in dilution. It is also interesting to see that the measured hardness of the SA weld metal is much lower than that for GTA weld metal, as shown in Figs. 3a and 5a, even though the cooling rate of SA weldment is approximately twice that of GTA weldment (Table 2). This trend is observed because the dilution for SA weld metal is relatively low ($D_1 = 0.45$, $D_2 = 0.24$, $D_3 = 0.15$) in comparison with GTA weld metal ($D_1 = 0.5$, $D_2 = D_3 = 0.27$), and the hardenability of the SA weld filler ($C_{eq} = 0.17$) is also lower than that of the GTA weld filler ($C_{eq} = 0.22$). In such a case, the tendency for the SA weld metal to form martensite at high cooling rates is constrained by the chemical-driven promotion of other ferritic phases (e.g. bainite and/or ferrite) [24].

The hardness predictions are in overall good agreement with experimental measurements for the three GTA weld samples (Figs. 3 and 4), despite the approximation that the experimentally observed acicular ferrite in GTA weld metal is treated as bainite in the FE weld model [24]. This agreement confirms that the approximation of acicular ferrite to bainite in the GTA weld model is acceptable from metallurgical point of view, as long as the microstructure of the GTA weld metal is a mixture of acicular ferrite, bainite and martensite [24]. In contrast, the SA weld model significantly overestimates the weld-metal hardness, although the hardness prediction for base-material HAZ is good (except for the over-tempered region [9]), as shown in Figs. 5 and 6. Experimental observations show that the microstructure of the SA weld metal is largely acicular ferrite with presence of some martensite-austenite islands and allotriomorphic ferrite [24]. Therefore, the inaccuracy of hardness prediction for the SA weld metal can be attributed to an unacceptable approximation of acicular ferrite to bainite in this case. Although acicular ferrite is broadly similar to bainite in terms of transformation temperature ranges [27,42] and it is widely regarded as intragranularly nucleated bainite [42,43], the growth of acicular ferrite is normally faster than that of bainite [42,44]. It is thus unsurprising that the present SA weld model underestimates bainite (or acicular ferrite) and overestimates martensite [24], leading to the overestimate of hardness in weld metal. In future work, more accurate SSPT kinetics for acicular ferrite should be incorporated in the metallurgical model to improve the prediction.

The residual stress analysis presented here is mainly qualitative for understanding dilution effect. The limitations can be attributed to following factors. First, the accuracy of the prediction about residual stress by a 2D weld model is limited by the 2D simplification [23,41]. Second, the present weld model adopted the mechanical properties of base material (i.e. SA508 Gr. 3 Cl. 1 steel) and its transformation products [30], which may not be fully representative for the weld metal [12]. Third, acicular ferrite in the weld metal has not been explicitly taken into account in the weld model. Despite these limitations, the following dilution effects have been identified for understanding the dominant trends, which are consistent with the findings of a previous study on dilution effects for a 20 mm thick GTA weldment [23]. Dilution affects residual stresses in both the FZ and HAZ (Figs. 7–10) of the GTA and SA weldments, via its effect on weld-metal SSPT kinetics. Specifically, dilution causes impacts on the phase-dependent mechanical properties and SSPT-induced strain experienced by the weld metal. For the mechanical properties, it is straightforward to understand that the residual stress level is limited by the yield strength of the final transformation products such as ferrite, bainite and martensite. For the transformation-induced deformation, the residual stresses in the as-deposited and reheated weld metals tend to be less tensile (or more compressive) in the 3-pass GTA and SA weldments when dilution is assumed to be one (i.e. purely base material), relative to the case when dilution is assumed to be zero (i.e. purely filler material), as shown in Figs. 7–10. Low temperature SSPT, particularly martensite transformation, is responsible for this mechanical behaviour. It is well known

that martensite transformation can effectively reduce tensile stresses at the locations wherein such transformation occurs [17,30,45–47]. As tensile residual stresses are produced by the constraint of thermal contraction during cooling, the metallurgical expansion associated with austenite decomposition can reduce the tensile stress through counteracting the thermal contraction. The compensation for thermal deformation is most effective when the start and finish temperatures of phase transformation are close to room temperature. Such a mechanism has been widely recognised [1,17,30,45,47]. Dilution plays an important role in this mechanism. For the studied weldments, the base material has highest hardenability and consequently martensite transformation is promoted in the weld metal with dilution increasing. Given a single transformation, according to the estimate using the chemical composition [30], the base material, GTA and SA weld fillers have martensite start temperatures of 406, 433 and 456 °C, respectively, and bainite start temperatures of 537, 555 and 579 °C, respectively. For multiple transforations, the transforamtions occur at lower temperatures for the base material than for the weld fillers (Fig. 1). Therefore, the start temperatures for phase transformations upon cooling are reduced in the weld metal with dilution increasing, thereby enhancing the effect of deformation compensation caused by austenite decomposition (the differences in metallurgical deformation between the base and filler materials have been demonstrated in Fig. 1). This effect is operative in both the as-deposited and reheated weld metals.

Based on the SSPT effect on residual stress, low transformation temperature filler alloy has been recently recommended for reducing tensile residual stress in weld metal [17,20,47]. In the stress engineered weldment, the martensite start temperature is controlled by high alloy filler and thus the dilution should be minimised. In contrast, for the weldments studied here, the relatively low martensite-start-temperature of the base material, as compared to the used fillers, means that high dilution is desirable for the purpose of tensile residual stress reduction in the weld metal. The effect of dilution on residual stresses in base-material HAZ is complicated, resulting from the balancing of the weld-metal stresses which are affected by dilution. The differences in the residual stresses and the associated dilution effect between GTA and SA weldments can be attributed to the following factors. First, GTA and SA welding processes used different filler materials (Table 1) and experienced different pass-to-pass variation in dilution and cooling rate (Table 2). Second, as the GTA welding process used in this study is relatively symmetric, compared against the SA welding process (Fig. 2), the different arrangements of weld bead deposition also affect the residual stress generated.

5. Concluding remarks

Effects of dilution on hardness and residual stresses in multipass weldments have been investigated for GTA and SA welding processes in grooved SA508 steel plates. A thermal-metallurgical-mechanical model with consideration of pass-to-pass variation in dilution has been developed to better understand dilution effects. Numerical predictions of hardness and residual stress are in reasonable agreement with measurements, despite some limitations of the weld model (e.g. 2D simplification and approximated kinetics of acicular ferrite transformation). Both the experimental observations and modelling results show that dilution can significantly influence both the weld-metal hardness and the residual stresses in FZ and HAZ. The sensitivity of these properties to the dilution effect is proportional to the differences in hardenability and SSPT between the base and filler materials used.

For the as-deposited and reheated weld metals studied here, increased dilution leads to higher hardness and lower tensile stresses (or higher compressive stresses) in both GTA and SA weld metals. This trend is observed because the base material is more prone to martensite formation at low temperature relative to the filler materials used. Hardness and residual stress values in the reheated weld metal are different from those in the as-deposited weld metal, owing primarily to the differences in dilution and thermal conditions. The transverse stresses do not appear to be as sensitive to dilution relative to the longitudinal stresses; this trend is likely due to the relative lack of constraint in the transverse direction. Although the properties of base material and its transformation products are not affected by dilution, residual stresses in the base material and HAZ can be appreciably affected by dilution as a result of a variation in balancing stresses imposed by the adjacent weld metal, which has been shown to be sensitive to dilution.

Declaration of competing interest

The authors have no conflict of interest to declare.

Acknowledgements

Research funding support from EPSRC grant EP/J021172/1, for the development and characterisation of welds under the NNUMAN programme, is acknowledged, and the EPSRC Fellowship in Manufacturing, EP/L015013/1, is also acknowledged. The authors are also grateful to J. Balakrishnan, P. English, M. Roy and I. Winstanley for their technical aid in weldment production and experimental measurement.

References

[1] J.A. Francis, H.K.D.H. Bhadeshia, P.J. Withers, Welding residual stresses in ferritic power plant steels, Mater. Sci. Technol. 23 (2007) 1009–1020.
[2] P. Withers, Residual stress and its role in failure, Rep. Prog. Phys. 70 (2007) 2211.
[3] S.J. Zinkle, G.S. Was, Materials challenges in nuclear energy, Acta Mater. 61 (2013) 735–758.
[4] P.R. Hurrell, D. Everett, A. Gregg, S. Bate, Review of residual stress mitigation methods for application in nuclear power plant, Proceedings of PVP (2006) 801–812.
[5] B. Energy, Assessment of the integrity of structures containing defects, R6 Revision 4 (2001) 155–169.
[6] M.C. Smith, A.N. Vasileiou, D.W. Rathod, J. Francis, N. Irvine, Y. Sun, A review of welding research within the new nuclear manufacturing (NNUMAN) programme, in: Proceedings of ASME 2017 Pressure Vessels and Piping Conference. Hawaii, USA, 2017.
[7] Y.L. Sun, C.J. Hamelin, T.F. Flint, A.N. Vasileiou, J.A. Francis, M.C. Smith, Prediction of dilution and its impact on the metallurgical and mechanical behavior of a multipass steel weldment, J. Pressure Vessel Technol. 141 (2019).
[8] Y.L. Sun, C.J. Hamelin, T.F. Flint, Q. Xiong, A.N. Vasileiou, I. Pantelis, J.A. Francis, M.C. Smith, Multi-pass ferritic steel weld modelling: phase transformation and residual stress, in: C. Sommitsch, N. Enzinger, P. Mayr (Eds.), Mathematical Modelling of Weld Phenomena, vol. 12, Verlag der Technischen Universität Graz, 2019, pp. 149–166.
[9] Y.L. Sun, G. Obasi, C.J. Hamelin, A.N. Vasileiou, T.F. Flint, J.A. Francis, M. C. Smith, Characterisation and modelling of tempering during multi-pass welding, J. Mater. Process. Technol. 270 (2019) 118–131.
[10] L. Shi, S.A. Alexandratos, N.P. O'Dowd, Prediction of prior austenite grain growth in the heat-affected zone of a martensitic steel during welding, Int. J. Pres. Ves. Pip. 166 (2018) 94–106.
[11] D.W. Rathod, Y. Sun, G. Obasi, M.J. Roy, Effect of multiple passes on Lüders/yield plateaus, microstructure and tensile behaviour of narrow-gap thick-section weld plates, J. Mater. Sci. 54 (2019) 12833–12850.
[12] A. Mark, J. Francis, H. Dai, M. Turski, P. Hurrell, S. Bate, J. Kornmeier, P. Withers, On the evolution of local material properties and residual stress in a three-pass SA508 steel weld, Acta Mater. 60 (2012) 3268–3278.
[13] S. Kou, Welding Metallurgy, John Wiley & Sons, New Jersey, 2003.
[14] T. Wang, A continuum damage model for ductile fracture of weld heat affected zone, Eng. Fract. Mech. 40 (1991) 1075–1082.
[15] D. Deng, H. Murakawa, Influence of transformation induced plasticity on simulated results of welding residual stress in low temperature transformation steel, Comput. Mater. Sci. 78 (2013) 55–62.
[16] D. Deng, H. Murakawa, Prediction of welding residual stress in multi-pass butt-welded modified 9Cr–1Mo steel pipe considering phase transformation effects, Comput. Mater. Sci. 37 (2006) 209–219.
[17] S.W. Ooi, J.E. Garnham, T.I. Ramjaun, Review: low transformation temperature weld filler for tensile residual stress reduction, Mater. Des. 56 (2014) 773–781.
[18] A. Hunt, A. Kluken, G. Edwards, Heat input and dilution effects in microalloyed steel weld metals, Welding J. New York- 73 (1994) 9–15.
[19] L. Halbauer, A. Buchwalder, R. Zenker, H. Biermann, The influence of dilution on dissimilar weld joints with high-alloy TRIP/TWIP steels, Weld. World 60 (2016) 645–652.
[20] T. Ramjaun, H. Stone, L. Karlsson, J. Kelleher, S. Ooi, K. Dalaei, J. Rebelo Kornmeier, H. Bhadeshia, Effects of dilution and baseplate strength on stress distributions in multipass welds deposited using low transformation temperature filler alloys, Sci. Technol. Weld. Join. 19 (2014) 461–467.

[21] H. Dai, R. Moat, P. Withers, Modelling the interpass temperature effect on residual stress in low transformation temperature stainless steel welds, in: ASME 2011 Pressure Vessels and Piping Conference, American Society of Mechanical Engineers, 2011, pp. 1451–1458.
[22] D. Deng, H. Murakawa, Finite element analysis of temperature field, microstructure and residual stress in multi-pass butt-welded 2.25Cr–1Mo steel pipes, Comput. Mater. Sci. 43 (2008) 681–695.
[23] Y. Sun, C.J. Hamelin, M.C. Smith, A.N. Vasileiou, T.F. Flint, J.A. Francis, Modelling of Dilution Effects on Microstructure and Residual Stress in a Multi-Pass Weldment. ASME 2018 Pressure Vessels and Piping Conference, American Society of Mechanical Engineers, Prague, Czech Republic, 2018.
[24] Y.L. Sun, G. Obasi, C.J. Hamelin, A.N. Vasileiou, T.F. Flint, J. Balakrishnan, M. C. Smith, J.A. Francis, Effects of dilution on alloy content and microstructure in multi-pass steel welds, J. Mater. Process. Technol. 265 (2019) 71–86.
[25] H. Wang, W. Woo, D.-K. Kim, V. Em, S.Y. Lee, Effect of chemical dilution and the number of weld layers on residual stresses in a multi-pass low-transformation-temperature weld, Mater. Des. 160 (2018) 384–394.
[26] E.J. Pavlina, C.J. Van Tyne, Correlation of yield strength and tensile strength with hardness for steels, J. Mater. Eng. Perform. 17 (2008) 888–893.
[27] H.K.D.H. Bhadeshia, Modelling of steel welds, Mater. Sci. Technol. 8 (1992) 123–133.
[28] Ş. Talaş, The assessment of carbon equivalent formulas in predicting the properties of steel weld metals, Mater. Des. 31 (2010) 2649–2653.
[29] P.V. Grant, J.D. Lord, P.S. Whitehead, The Measurement of Residual Stresses by the Incremental Hole Drilling Technique, National Physical Laboratory, 2002.
[30] C.J. Hamelin, O. Muránsky, M.C. Smith, T.M. Holden, V. Luzin, P.J. Bendeich, L. Edwards, Validation of a numerical model used to predict phase distribution and residual stress in ferritic steel weldments, Acta Mater. 75 (2014) 1–19.
[31] P. Maynier, J. Dollet, P. Bastien, Creusot-Loire system for the prediction of the mechanical properties of low alloy steel products, in: D.V. Doane, J.S. Kirkaldy (Eds.), Hardenability Concepts with Applications to Steels, The Metallurgical Society of AIME, Warrendale, Pennsylvania, 1978, pp. 518–545.
[32] M.V. Li, D.V. Niebuhr, L.L. Meekisho, D.G. Atteridge, A computational model for the prediction of steel hardenability, Metall. Mater. Trans. B 29 (1998) 661–672.
[33] C. Henwood, M. Bibby, J. Goldak, D. Watt, Coupled transient heat transfer—microstructure weld computations (Part B), Acta Metall. 36 (1988) 3037–3046.
[34] C.J. Hamelin, O. Muránsky, L. Edwards, The influence of austenite grain size during welding simulations of ferritic steels, Adv. Mater. Res. 996 (2014).
[35] J. Kirkaldy, D. Venugopalan, Prediction of microstructure and hardenability in low-alloy steels, Phase Trans. Ferr. Alloy. (1983) 125–148.
[36] A.A.B. Sugden, H.K.D.H. Bhadeshia, A model for the strength of the As-deposited regions of steel weld metals, Metal. Trans. A 19 (1988) 1597–1602.
[37] G. Greenwood, R. Johnson, The deformation of metals under small stresses during phase transformations, in: Proceedings of the Royal Society of London A: Mathematical, Physical and Engineering Sciences, vol. 283, The Royal Society, 1965, pp. 403–422.
[38] C.L. Magee, H.W. Paxton, Transformation Kinetics, Microplasticity and Aging of Martensite in Fe-31 Ni, DTIC Document, 1966.
[39] A.N. Vasileiou, M.C. Smith, J. Balakrishnan, J.A. Francis, C.J. Hamelin, The impact of transformation plasticity on the electron beam welding of thick-section ferritic steel components, Nucl. Eng. Des. 323 (2017) 309–316.
[40] J.-B. Leblond, G. Mottet, J. Devaux, J.-C. Devaux, Mathematical models of anisothermal phase transformations in steels, and predicted plastic behaviour, Mater. Sci. Technol. 1 (1985) 815–822.
[41] S. Sarkani, V. Tritchkov, G. Michaelov, An efficient approach for computing residual stresses in welded joints, Finite Elem. Anal. Des. 35 (2000) 247–268.
[42] S.S. Babu, The mechanism of acicular ferrite in weld deposits, Curr. Opin. Solid State Mater. Sci. 8 (2004) 267–278.
[43] G.I. Rees, H.K.D.H. Bhadeshia, Thermodynamics of acicular ferrite nucleation, Mater. Sci. Technol. 10 (1994) 353–358.
[44] S.S. Babu, S.A. David, Inclusion formation and microstructure evolution in low alloy steel welds, ISIJ Int. 42 (2002) 1344–1353.
[45] H. Dai, J. Francis, P. Withers, Prediction of residual stress distributions for single weld beads deposited on to SA508 steel including phase transformation effects, Mater. Sci. Technol. 26 (2010) 940–949.
[46] J.A. Francis, M. Turski, P.J. Withers, Measured residual stress distributions for low and high heat input single weld beads deposited on to SA508 steel, Mater. Sci. Technol. 25 (2009) 325–334.
[47] J.A. Francis, H.J. Stone, S. Kundu, H.K.D.H. Bhadeshia, R.B. Rogge, P.J. Withers, L. Karlsson, The effects of filler metal transformation temperature on residual stresses in a high strength steel weld, J. Pressure Vessel Technol. 131 (2009), 041401-041408.